Applied Surface Science 508 (2020) 145143

Contents lists available at ScienceDirect

Applied Surface Science

journal homepage: www.elsevier.com/locate/apsusc

Full Length Article

Laser-assisted modification of titanium dioxide nanotubes in a tilted mode as surface modification and patterning strategy

Jakub Wawrzyniak[a,*], Jakub Karczewski[b], Piotr Kupracz[a], Katarzyna Grochowska[a], Karol Załęski[c], Oleksandr Pshyk[c], Emerson Coy[c], Michał Bartmański[d], Marek Szkodo[d], Katarzyna Siuzdak[a]

[a] Centre for Plasma and Laser Engineering, The Szewalski Institute of Fluid-Flow Machinery, Polish Academy of Sciences, Fiszera 14 St., 80-231 Gdańsk, Poland
[b] Faculty of Applied Physics and Mathematics, Gdańsk University of Technology, Narutowicza 11/12 St., 80-233 Gdańsk, Poland
[c] NanoBioMedical Centre, Adam Mickiewicz University, Wszechnicy Piastowskiej 3, 61-614 Poznań, Poland
[d] Faculty of Mechanical Engineering, Gdańsk University of Technology, Narutowicza 11/12 St., 80-233 Gdańsk, Poland

ARTICLE INFO

Keywords:
Laser irradiation
TiO_2 nanotubes
Phase conversion
Surface patterning
Optical properties

ABSTRACT

Electrochemical anodization is regarded as a facile and easily scalable fabrication method of titania nanotubes (TiO_2NTs). However, due to the extended duration of calcination and further modifications, much faster alternatives are highly required. As a response to growing interest in laser modification of nanotube arrays, a comprehensive investigation of pulsed-laser irradiation and its effect onto TiO_2NT properties has been carried out. The impact of irradiation onto the surface being placed at different angles in respect to the laser beam was studied and evaluated. The usage of the motorized table enables formation of laser-treated traces over the selected area. SEM and TEM analysis provides insight into morphological changes and shows partial melting of nanotubes surface, which is accompanied by the decrease of internal TiO_2 tube diameter just below the melted region. Although structural and optical analysis consisting of Raman, photoluminescence and UV–Vis data indicate that presented method does not result in complete material crystallization, it promotes creation of advantageous localized states within TiO_2 bandgap that may play a crucial role in charge separation. Moreover, impressive improvements to the mechanical properties resulting from the laser-modification are presented.

1. Introduction

The titanium dioxide nanotubes (TiO_2NTs) without a doubt can be included in the group of the most investigated functional nanomaterials since the number of paper dedicated to them increases at an impressive rate [1]. They are typically obtained via electrochemical oxidation of titanium foil and their properties are highly dependent on morphology, such as their final length [2], spacing [3] or pore size [4]. However, they can be relatively easily tailored by adjusting anodization parameters and electrolyte composition. Owing it to easily controlled fabrication and quite low equipment requirements, TiO_2NTs have found a lot of success in research involving photocatalysis [5], solar cells [6], filtering systems [7], and gas sensors [8]. However, as it is known, as-anodized TiO_2NTs are in the amorphous phase, limiting their immediate usability. In order to obtain crystalline material, they are usually annealed in a furnace in about 450 °C for at least one hour. Nevertheless, considering heating and cooling time, the whole process can take up a whole working day. Thus, the main drawback of this method is the heat treatment duration to achieve crystalline phase, while the size of the material placed in the oven is limited by its dimensions.

As an alternative to traditional calcination process, low-temperature approaches towards phase transition have been proposed in the literature. Until now, successful crystallization of TiO_2NTs was reported using plasma [9] and vapour treatment [10], alternating voltage [11] and transmission electron microscope (TEM) [12]. According to Yu et al. [10], different methods used for phase transformation exhibit a great influence onto the crystallinity, morphology, architecture as well as photoactivity and the biological response of TiO_2NTs layer. Therefore, it should be kept in mind that the change of phase is not the only result of the particular treatment of as-anodized titania nanotubes. Recently published results reporting on plasma-assisted approach [9], show that such conditions induce crystallization within only a few seconds of exposure to oxygen plasma, without changing the morphology of NTs. At the certain plasma conditions, namely, forward power of 800 W applied only for 1 s is sufficient for reaching anatase

* Corresponding author.
E-mail address: jwawrzyniak@imp.gda.pl (J. Wawrzyniak).

https://doi.org/10.1016/j.apsusc.2019.145143
Received 9 July 2019; Received in revised form 12 December 2019; Accepted 19 December 2019
Available online 23 December 2019

phase, but the temperature of the whole sample rapidly increases up to 1030 °C, while the maintenance of temperature below 1000 °C at lower plasma power does not ensure crystallization. Consequently, for a successful phase transition, the whole substrate is treated at a much more elevated temperature than in the furnace. In the case of water vapour treatment [13], as the exposure exceeds 30 min, NTs finally convert into the porous rod-like structure along with a significant change in the recorded FTiR, Raman and UV–vis spectra. Other method concerns the immersion of Ti foil covered by TiO_2NTs in water at 92 °C for over 6 h and results indicate that water plays a crucial role in the rearrangement processing of the TiO_6^{2-} octahedral. As Liao et al. [14] reported, during hot water treatment the surface roughness increases and the initially ordered morphology is not observed anymore. Unfortunately, upon sample immersion, the tubular layer peels off the substrate and is finally used in the form of powder for photocatalytic degradation tests. It should be also underlined, that those methods are difficult to scale-up since dimensions of water batch chamber and furnace are limited. Moreover, regardless of the dimensions of the samples and their number designated to simultaneous treatment, the cost of larger size equipment itself increases significantly. On the contrary to above-described methods, laser irradiation has been proposed as an easy, fast and scalable way of inducing phase transition in TiO_2NTs as well as surface modification. In the past, laser treatment was used towards crystallization of thin layers [15,16] as well as welding the interface between TiO_2 and fluoride tin oxide electrode towards DSSC efficiency improvement [17]. Following promising results on flat titania surface, a laser beam was applied for tubular layer treatment. Nevertheless, there have been only few reports describing changes of morphology, structure or properties of the nanotubes. Xu et al. [18] proved that melting of upper parts of the anatase NTs layer upon laser irradiation occurs and impacts significantly their photoelectrochemical response.

On the contrary, Hsu et al. [19] focused on the annealing of amorphous nanotubes. The process was performed when the samples were rotated in order to homogenize modified surface. During the rotation, simultaneous tilt mode was applied to improve crystallinity across the NTs layer since the penetration depth of the laser beam is limited. Nevertheless, further materials characterization concerned only analysis of topography and crystalline phase of some selected samples. Moreover, application of the sample rotation enabling uniform surface modification still cannot be applied for larger substrates or those exhibiting irregular shape.

In order to overcome listed problems, arising when conventional calcination is performed or laser treatment within a small area is carried out, herein we propose laser irradiation of as-anodized titania, where the sample is moving relative to the beam. Such an approach enables laser beam scanning along the precisely determined path and in consequence modification over an area of any shape and size. A homogeneous modification was achieved by moving TiO_2NT substrate located at the motorized stage both in the perpendicular plane and under tilted mode in respect to the direction of the laser beam. Such an approach affects the size of the laser spot since its area grows with increasing angle between the beam and the substrate. We present a comprehensive analysis of physical and morphological changes induced in amorphous TiO_2NTs by nanosecond UV laser irradiation. While morphological transformations were captured by SEM both at the surface and at the cross-section of the material, certain topographical features were better visualized through TEM imaging. The change in crystallinity was observed using Raman spectroscopy and optical properties were discussed based on UV–Vis and photoluminescence measurements. Moreover, the mechanical properties of reference and modified material were determined via nanoindentation, as it has been shown that pillars covered by TiO_2 can endure stress well and show improved mechanical properties under certain conditions [20].

2. Experimental

2.1. Sample preparation

Ordered titanium dioxide nanotubes were synthesized by the means of electrochemical oxidation carried out in the cylinder shape electrochemical cell with an outer jacket. First, titanium foil (99.7%, Strem) was cut into 35 × 25 mm pieces and cleaned ultrasonically for 10 min in acetone (p. a. Protolab), ethanol (96%, Chempur) and deionized water (0.08 μS, Hydrolab), respectively. After drying in air, the foil was used as a working electrode in the anodization process, while platinum net (20 × 25 mm) acted as a counter electrode. The electrolyte solution contained 9.2 wt% NH_4F (p. a. Chempur), 15 vol% deionized water and 85% of ethylene glycol (p.a. Chempur). The procedure was performed in 23 °C (controlled by thermostat Julabo F-12), under 40 V for 45 min. Ramp-up and ramp-down voltages were set to 0.1 V/s and controlled by in-house built hardware equipped with a constant voltage generator (MPS-600-5L-2) and precisely adjusted using dedicated software. After the process, the foil was rinsed with and submerged in ethanol for 1 h, after which it was left to dry in air. Substrates obtained that way underwent thermal treatment in the pulsed and continuous mode.

Laser modification of the TiO_2NTs was performed using Nd:YAG pulsed laser (6 ns, Quantel), equipped with 4th harmonics generator crystals (λ = 266 nm) and set to 2 Hz pulse repetition rate. The laser beam was homogenized and focused on the surface of the sample, creating a 2.4 × 2.4 mm spot at 0° angle of incidence (AOI). The fluence of laser pulse was changed between 25 and 75 mJ/cm^2 and measured by Coherent FieldMaxII Top radiometer. The sample was placed onto the computer-controlled 4-axis stage (SmarAct) moving precisely during the whole modification process. The tilted mode applied to the motorized table enables change of the angle between the plane of the sample surface and the incident laser beam. Following that, the angle was increased from 0° to 80°, changing the area exposed to the laser radiation. It should be noted, that with increased angle of irradiation, the spot size grows from 2.4 up to 14.1 mm, following inversely cosine of the angle of incidence ($a = a_0/\cos\theta$). In accordance with this change, the laser fluence was established. At each angle, the sample moved along the axis parallel to the shorter spot edge at a constant speed of 3.5 mm/min two times - back and forth. The whole process was performed in ambient conditions.

Continuous thermal treatment was carried out in order to obtain the reference sample. It was prepared with the use of electric furnace (Nabertherm) in 450 °C for 2 h with the heating rate set to 2 °C/min. Cooling down was performed freely to the room temperature. The whole process takes over 14 h, including heating up and cooling down.

2.2. Characterisation

Scanning Electron Microscope pictures were taken with FE-SEM, FEI Quanta FEG 250 equipped with a secondary electron detector. The SEM images were taken at the surface, at the cross-section, and in different places of the sample surface to confirm its uniformity.

TEM images were taken using JEOL ARM 200F transmission electron microscope working at 80 kV. TiO_2NTs were prepared by Focus Ion Beam (FIB) using a JEOL JIB-4000 instrument, with Ga ion source at different voltages (3–30 kV). Cross-sections were placed on commercially available Cu grids for analysis.

Raman characterization was performed using Renishaw Raman spectrometer equipped with 514 nm argon ion laser with emission power of 50 mW. Measurements were taken using ×50 objective, 10 s exposure time and utilizing 10% of laser power in the range of 100–2000 cm^{-1}. The Raman spectra were collected in three different places of the sample, in the centre and towards vertical edges when titled mode was applied.

UV–Vis measurements were taken in reflectance mode with PerkinElmer dual-beam spectrophotometer in the range of

300–1100 nm. Scanning speed was set to 120 nm/min.

Photoluminescence (PL) spectra of the samples were measured at room temperature using a SHAMROCK - SR-303I-A Spectrograph (Andor Technology) equipped with a 450 mW LED as the excitation light source (λ = 365 nm) and ICCD camera as a detector. Optical filters, FGUV-11 (Thorlabs) and GG 400 (Schott AG) were used to eliminate undesired light modes during measurements of the PL excitation spectra. Overall, 200 scans in the range of 370–800 nm were collected and their sum was used for further evaluation.

Nanoindentation tests were performed with the NanoTest™ Vantage (Micro Materials) using a Berkovich three-sided pyramidal diamond. Fifteen independent measurements of indentation were carried out for each sample and two references specimens. One curve for a medium hardness was selected for analysis. The maximum applied force was equal to 0.45 mN, the loading time was set up at 5 s, the dwell period at maximum load was 2 s and unloading time was set up at 5 s. The distances between the subsequent indents were 20 μm. Based on the load–penetration curves and used the Oliver and Pharr method, surface hardness (H) and reduced Young's modulus (E) were calculated using the integrated software.

3. Results and discussion

3.1. Morphology

Fig. 1A and 1C present SEM images of as-anodized TiO_2 nanotubes, while Fig. 1B and 1D show furnace annealed sample used here as a reference one. According to the top and cross-section images, the geometrical parameters could be determined. The nanotube length was ca. 2.1 μm with the internal diameter of 100 nm, whereas wall thickness and spacing between crowns - of ca. 15 nm for both as-anodized and annealed samples.

The effects of differing angle and various laser fluences onto nanotubes are visualized in Figs. 2, 3, and 4 which confirm transformation of the surface morphology. Although in all cases some degree of surface melting is visible, the effect is stronger with increased pulse fluence. In the SEM image obtained for TiO_2NTs modified at the fluence of 25 mJ/cm^2 (Fig. 2A–C), some nanotubular morphology is still visible underneath thin melted layer, whereas for higher pulse fluences melted region tightly covers ordered architecture (Fig. 2D, E). Interestingly, different kind of structure emerges from the melted layer – uniform morphology enriched with micropores (Fig. 2G, H). Samples modified at higher angles of incidence (Fig. 2F, I), however, require significantly higher fluences in order to transform their morphology into structures similar to those obtained at lower angles.

After irradiation, the tubular structure shortened by 0.5, 0.8 and 1 μm, for laser fluences of 25, 50 and 75 mJ/cm^2, respectively (see Fig. 3). It is noteworthy that, in the intermediate region between nanotubes that are left intact and melted top layer, the nanotubes tend to form necks as presented in Fig. 4 A. Although the degree of contraction varies heavily, it narrows the width of each nanotube by about 50% and is likely caused by the upward material flow, towards the melted region. This effect is especially visible for the higher fluences with more developed melted region.

Introducing varying angle to the conversion process has a significant effect onto the final morphology, as illustrated in Figs. 2 and 3. As indicated in the experimental section, change in the incident angle influences the sample area exposed to the laser radiation. Although the difference between the length of melted nanotubes during modification is relatively small, transforming nanotubes at an angle decreased the total length of melted nanotubes by about 20%. This affects topological changes, which indicate that the surface of the samples modified at an

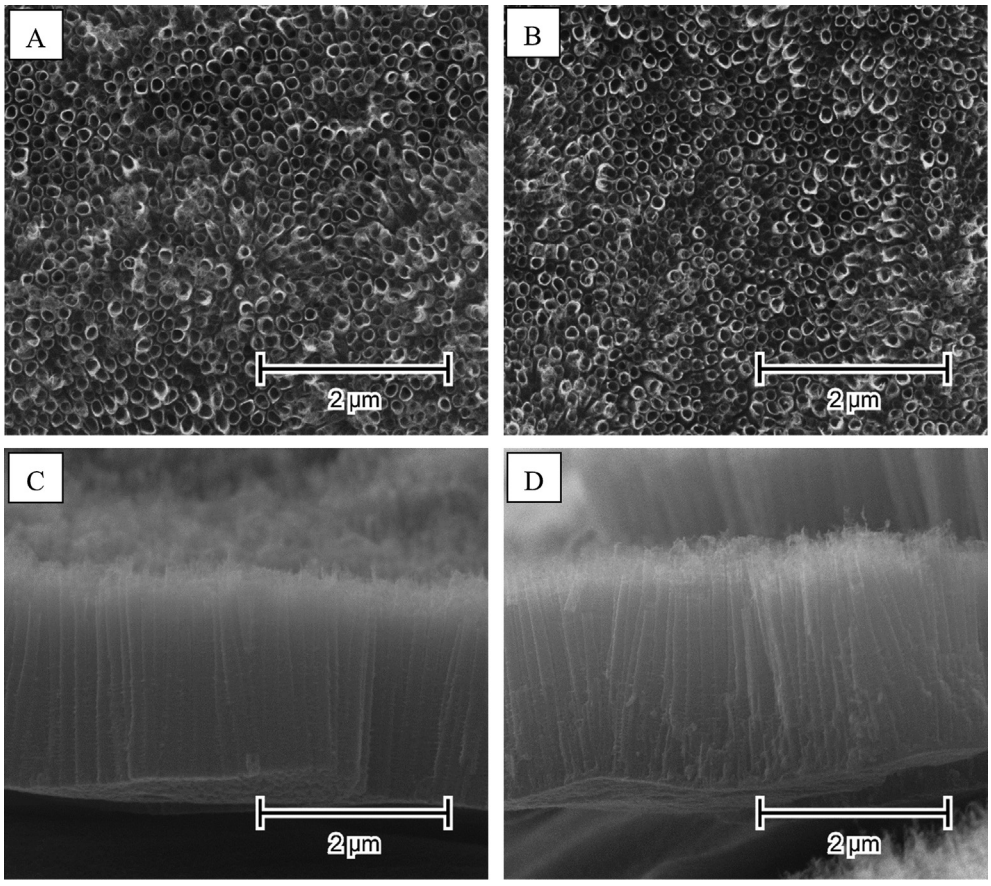

Fig. 1. SEM images of as-anodized (A) and furnace annealed (B) nanotube arrays along with their respective cross-sections (C, D).

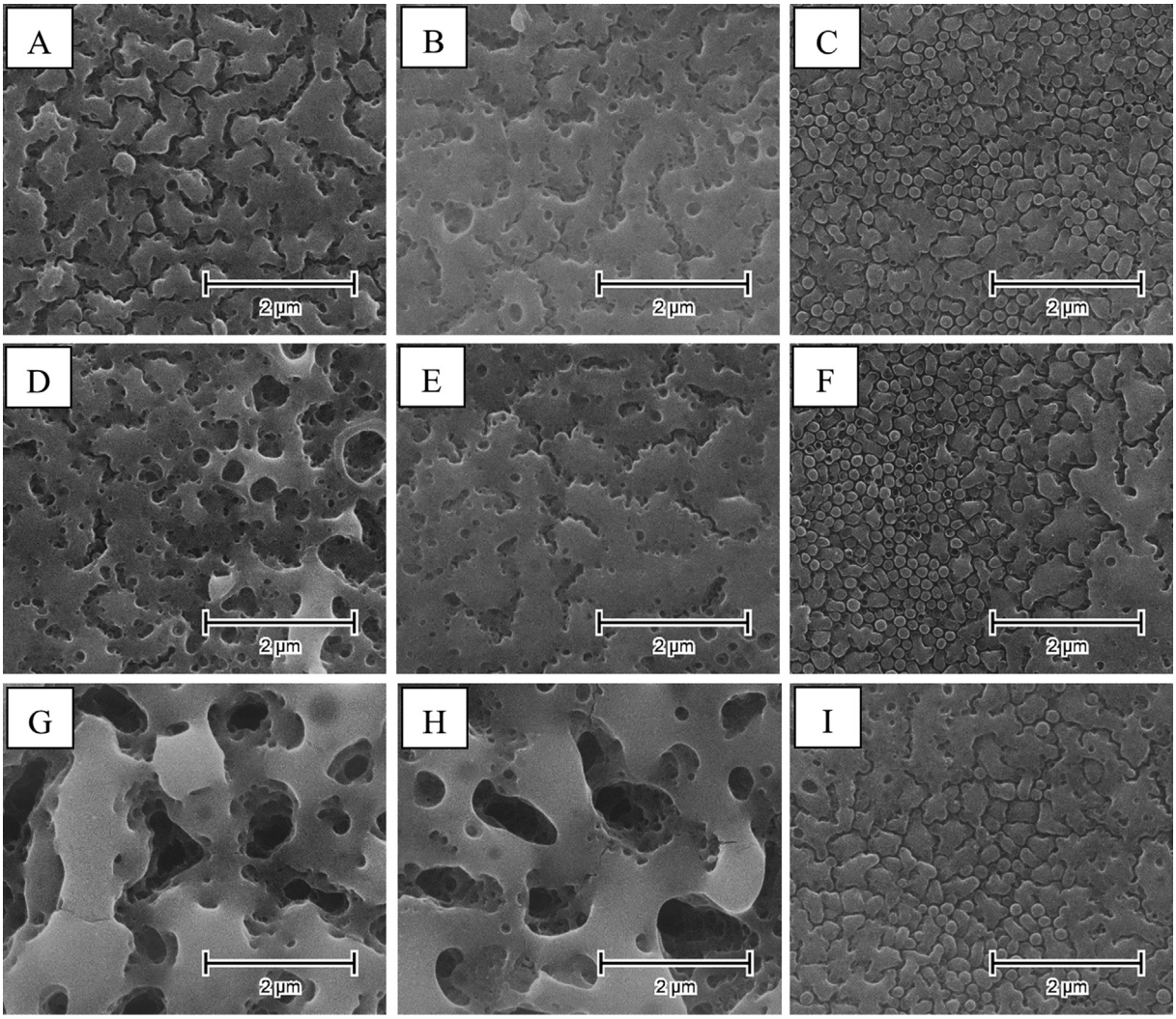

Fig. 2. SEM images of the modified TiO_2NT surfaces. First row (A–C) shows samples modified with pulses of 25, second (D–F) with 50 and third (G–I) with 75 mJ/cm^2, while columns represent angle at which samples were modified, from left: 0, 30, and 80° respectively.

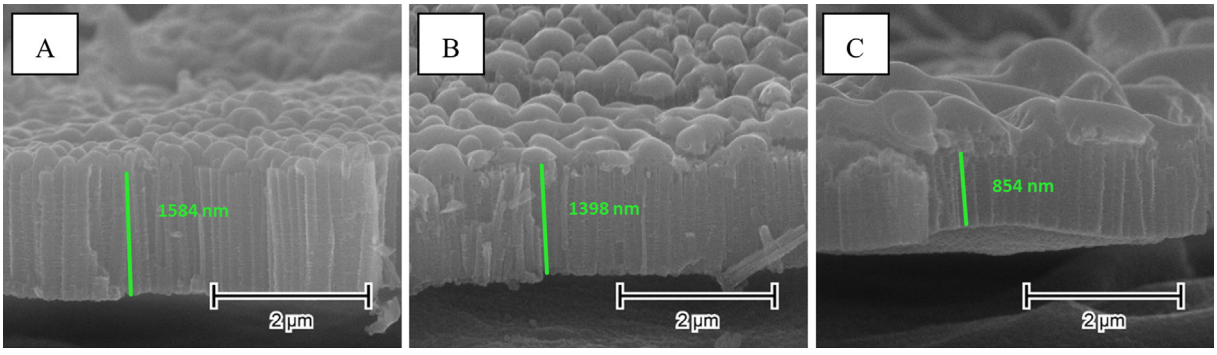

Fig. 3. Cross-sectional SEM images of laser-modified TiO_2NTs with 25 (A), 50 (B), and 75 (C) mJ/cm^2 laser pulses at the normal angle of incidence.

angle are much less transformed compared to the case when sample plane was perpendicular to the laser beam. Interestingly, the surface of tilted (80°) altered with pulses of 75 mJ/cm^2 represents similar degree of changes than non-tilted samples treated with 25 mJ/cm^2. In addition, modification in tilted mode results in a directional orientation of micropores due to non-uniform irradiation of any given nanotube, as presented in Fig. 4B, C. This effect was not observed by Hsu et al. [19], likely due to rotation incorporated into reported modification method. In the case of irradiation of tilted TiO_2NTs, substantially more light is being absorbed by the lower part of nanotubes inner wall than its outer wall on the opposite side, which is covered by lower wall of the neighbouring nanotube. This causes each nanotube to melt non-uniformly, resulting in the directional orientation of micropores visible in Fig. 4B.

3.2. Structure

Raman spectra were gathered from as-anodized, thermally annealed

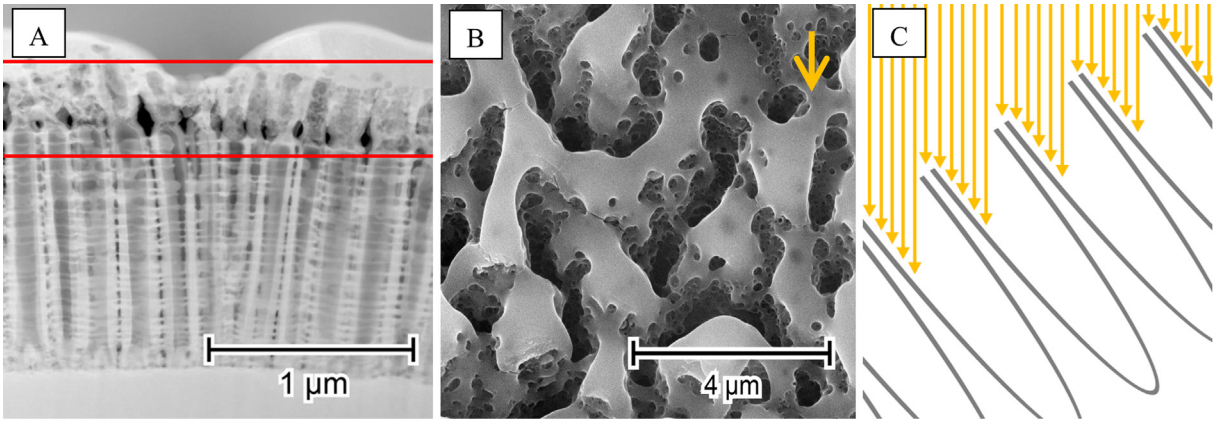

Fig. 4. TEM image of TiO_2NTs modified by 75 mJ/cm^2 laser pulses at the 30° angle of incidence with visible necks under melted top layer (A), directional orientation of transformed structure (B) with an arrow indicating direction of laser beam and visualisation of irregularities in irradiation of the nanotubes (C).

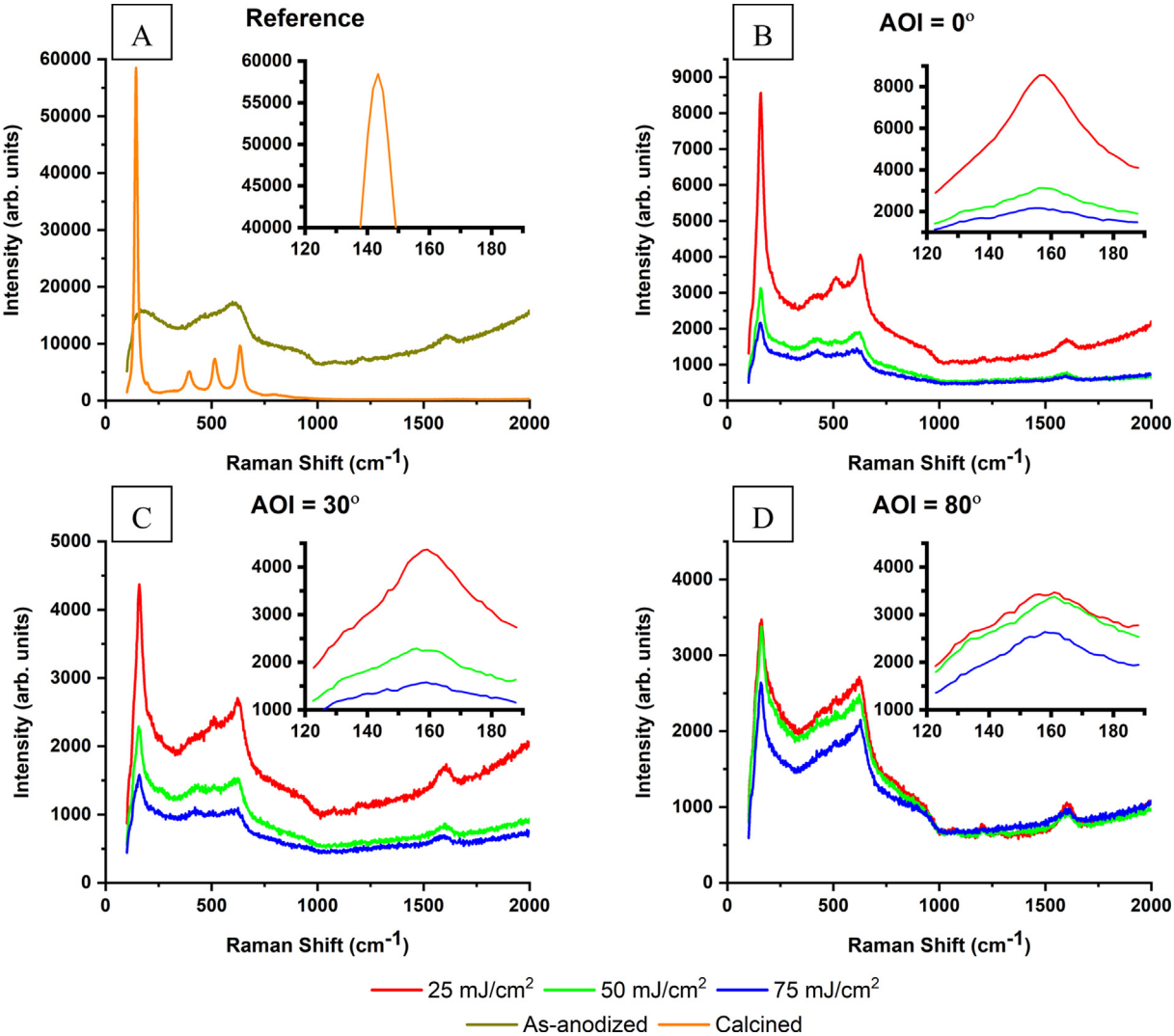

Fig. 5. Raman spectra for reference (A) samples and those modified at AOI = 0 (B), 30 (C), and 80° (D) with laser fluences of 25, 50, and 75 mJ/cm^2.

and laser-modified nanotube arrays and shown in Fig. 5. As-anodized titania nanotubes exhibit broad spectra without any clear peaks, which are characteristic for amorphous TiO_2 nanotubes [13,21,22]. Those wide humps appearing in the range of 120–310 cm^{-1} correspond to the Ti—O bending, while the band at 400–745 cm^{-1} comes from Ti—O stretching vibrations [23]. In Raman spectra of calcined material, clear maxima at 144 ($E_{g(1)}$), 197 ($E_{g(2)}$), 395 (B_{1g}), 519 (B_{1g}), and 635 ($E_{g(3)}$) cm^{-1} are visible, which are characteristic for anatase phase [24]. In addition, faint peak at about 1600 cm^{-1} was recorded which can be associated with the presence of amorphous carbon [25] originating from the thermal decomposition of the organic compound present in the electrolyte used for anodization. Presented results go in line with

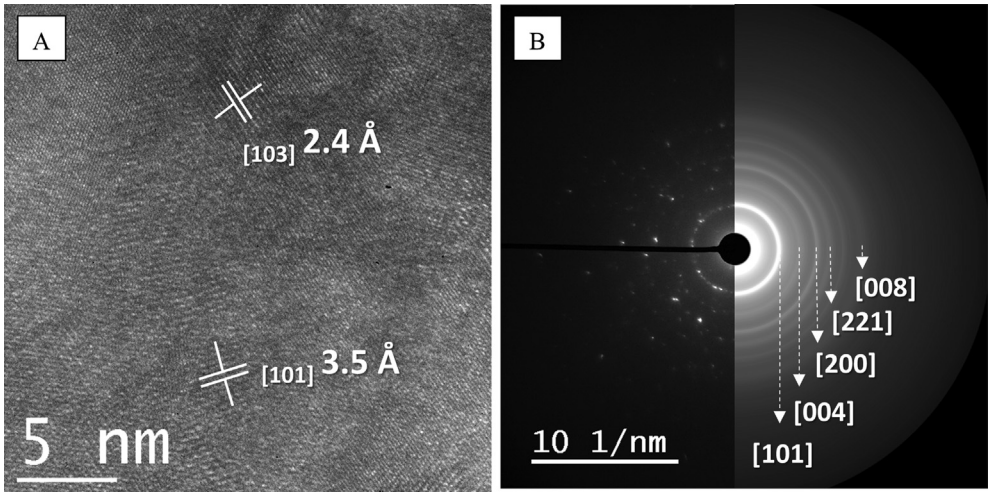

Fig. 6. The high resolution image of the TiO_2NTS surface, where multiple interplanar distances can be observed (A), and the processed diffraction pattern obtained by the Difftools pluging in Digital Micrograph [29] (B). All the indexed peaks correspond to the anatase phase of TiO_2.

those obtained by other investigators [13,22].

Although in laser-modified material all anatase peaks can be detected, their intensity decreases with increased fluence and the angle of modification. In addition, the $E_{g(1)}$ mode shifts towards 159 cm^{-1}, which indicates non-stoichiometric composition through i.e. presence of oxygen vacancies and is sometimes referred to as self-doping [26]. The signals attributed to the anatase phase become nearly undetectable for samples treated with 75 mJ/cm^2 for all modification angles. While lowering of the intensity could be explained by changes in surface geometry, the disappearance of anatase peaks might be associated with laser-induced disordering of the structure during rapid temperature changes [27,28]. The HR-TEM and SAED analysis confirms laser-induced partial crystallisation of TiO_2NTs to anatase, as shown in Fig. 6.

3.3. Optical properties

In order to derive bandgap values of the modified material, the UV–Vis absorption spectra were measured and Tauc plots for respective samples were prepared (Fig. 7). Indirect allowed transitions were assumed, which according to Tauc's relations are also valid for non-crystalline materials [30,31]. The typical bandgap value for TiO_2 found in the literature [14,32] is about 3.2 eV, however, the calculated value in both of our reference samples equals 3.15 eV. Because E_{bg} is the same for as-anodized and calcined material, the 0.05 eV lower value compared to other reports is likely due to the geometrical aspect of the nanotubes, which is preserved during calcination. E_{bg} values determined for each of laser-modified samples (Table 1) are significantly lower in comparison to thermally annealed titania NTs. In addition, samples modified using 50 mJ/cm^2 laser pulses tend to have significantly lower bandgap values, than the other investigated cases (Fig. 7B, C). As an exception, within samples modified at an 80° angle, the one modified with 75 mJ/cm^2 pulses had the lowest bandgap (Fig. 7D). Interestingly, those samples share similar morphology (see Fig. 2D, E, I), which indicates favourable modification parameters for the creation of localized states within the bandgap of the material [33]. This could potentially improve their photoactivity by i.e. allowing the material to absorb longer wavelengths.

In order to describe the optical and electronic properties of titania NTs, the photoluminescence measurements were performed. An example of the recorded photoluminescence (PL) spectrum of the sample treated with a fluence of 50 mJ/cm^2 at the normal angle of incidence is given in Fig. 8 B, whereas PL for the calcined titania NTS is presented in Fig. 8 A. Comparing both spectra, one may observe clear difference especially in the contribution of the blue emission. It shows the main maximum at around 530 nm with a strong shoulder on the low wavelength side and a long tail on the other. Taking into account resolved PL spectra reported by other authors [34–38], the distinctive emission bands should be found at around $\lambda_{blue} \approx$ 400–480 nm, $\lambda_{green} \approx$ 500–540 nm, and $\lambda_{red} \approx$ 590–660 nm. The most accurate deconvolution was performed using parameters listed in Table.

The blue photoemission could be attributed to recombination of electrons trapped in oxygen vacancies below the conduction band (CB) with mobile holes present in valence band [37]. Green photoluminescence might rely on the recombination of trapped holes on Ti^{3+} ions or conduction band electrons [36,38]. According to Pallotti et al. [38], excitation of red photoemission can be observed using below-bandgap activation, therefore, additional radiative channel involving trapped electrons should be present in the material which would be responsible for red photoemission between 600 and 650 nm.

Photoluminescence measurements spectra have shown that laser annealing of the TiO_2 nanotubes changes their emissivity and influences the shape of their spectrum. The strongest change relates to the emission of red light. As seen in Fig. 9 A, the lowest intensity of red emission is observed for the laser beam guided parallel to nanotubes grow direction and an increment of the angle is followed by the stronger red emission. On the other hand, the green emission is enhanced by the laser annealing and the laser beam angle is not relevant, what is shown in Fig. 9B. The blue photoemission in laser-modified samples is weaker than in reference samples and changes inversely with the angle of modification for samples modified with 50 and 75 mJ/cm^2 pulses (Fig. 9C).

While calcination leads to increased blue emissivity and decrement to green and red emissions, the laser treatment ensures lower emissions in red and blue range while simultaneously increasing green photoluminescence.

The increment of the green PL caused by the laser treatment indicates a growing number of holes trapped within the material, whereas lower emissions in red and blue suggest decreasing the number of Ti^{3+} ions and oxygen vacancies through which electrons dissipate energy in as-anodized TiO_2NTs. Schematic representation of the summary of PL mechanisms within the material is shown in Fig. 10.

3.4. Mechanical properties

In Fig. 11 it is possible to observe slight steps for both calcined and as-anodized nanotubes. They indicate that under the applied load, nanotubes first bend elastically and, as the depth increases, they break. Consequently, the material becomes denser, producing higher

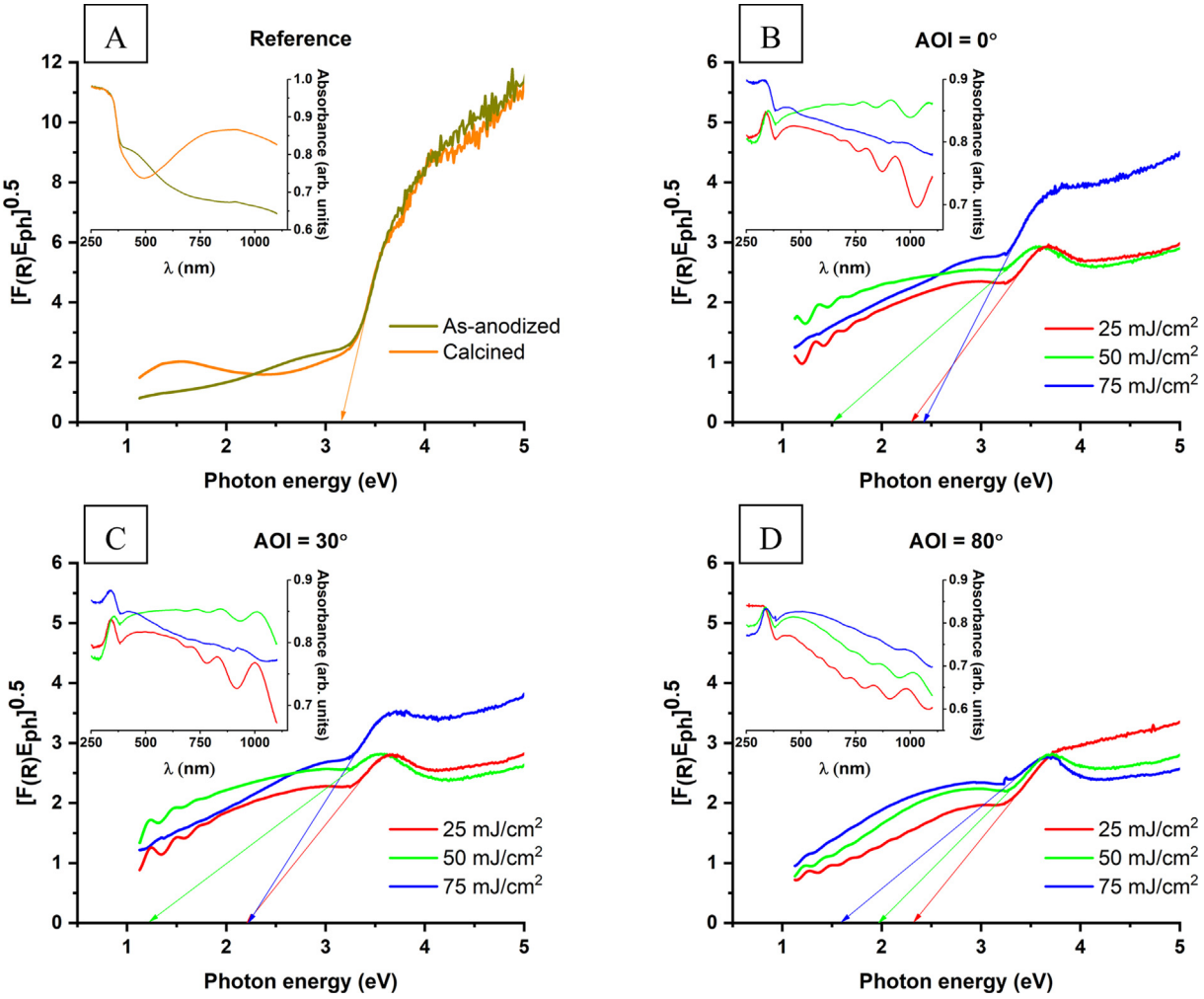

Fig. 7. Tauc plots calculated for reference samples (A) and samples modified at normal (B), 30° (C), and 80° (D) angles with different laser fluences. Included insets present absorbance of the respective samples.

Table 1
Band-gap values (in eV) calculated from Tauc plots presented in Fig. 7.

Fluence	Angle		
	0°	30°	80°
25 mJ/cm^2	2.30	2.21	2.32
50 mJ/cm^2	1.50	1.21	1.96
75 mJ/cm^2	2.42	2.22	1.59

resistance that grows with indentation depth.

Amorphous TiO_2NTs show higher hardness and reduced Young's modulus in comparison to calcined TiO_2NTs. The latter relation is in agreement with other reports [39], as amorphous materials tend to have higher hardness and elasticity modulus than their crystalline counterparts.

Some parameters of laser treatment show vastly improved mechanical properties in comparison with the reference samples. Table 3 presents results of nanoindentation tests. As can be seen from the results in Table 3, almost all laser machining methods have increased hardness in comparison to calcined TiO_2NTs (Table 3). In some cases, laser processing also increased the hardness and elasticity modulus in comparison with amorphous nanotubes obtained after anodization. A particularly visible increase in hardness and elastic modulus occurred after remelting under the highest fluence of 75 mJ/cm^2 and for 80° angle. This mode of laser processing yielded more than three-fold increase in hardness and over 50% increase in the elastic modulus in comparison with amorphous TiO_2 nanotubes. The increase of mechanical properties after laser treatment can be associated with a higher dislocation density and compressive residual stress caused by laser remelting. In addition, the hysteresis loop for each sample has been recorded (Fig. 11), indicating their ability to dissipate energy elastically [39,40].

4. Conclusions

In summary, we have demonstrated the effects of laser-treatment onto TiO_2 nanotube arrays, considering different modification angles. Angle- and fluence-dependent changes onto morphology were described and discussed along with, structural, and mechanical properties induced through laser irradiation. We have found that upon laser radiation top part of titania nanotubes has become porous at the expense of the thickness of an ordered tubular layer. Additionally, samples subjected to higher-energy pulses, which exhibit appreciable melted region, have a very clear contraction in their diameters in the region adjacent to the melted area. Particularly important is that such modification can be done in a precisely defined area and angle through the use of a motorized table. Although laser-treatment alone is not sufficient for phase transition of the whole titania layer material, it promotes the creation of advantageous localized states within band-gap of the material. Among others, titania NTs treated with 75 mJ/cm^2 laser pulses show superior mechanical properties compared to both amorphous and calcined samples.

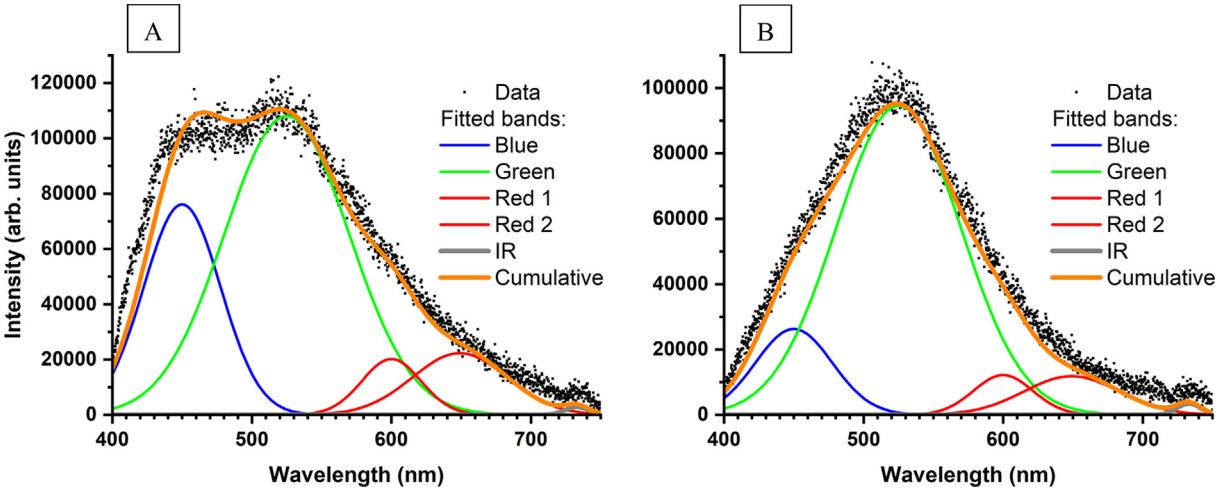

Fig. 8. Deconvoluted photoluminescence spectra of calcined TiO_2NTs (A) and NTs modified with 50 mJ/cm^2 laser pulses at 30° angle of incidence (B).

Table 2
The fitting parameters used to perform deconvolution of photoluminescence spectra given in Fig. 8, recorded for sample modified with 50 mJ/cm^2 at 0°.

Colour	Peak position (nm)	FWHM (nm)
Blue	450	65
Green	525	105
red 1	600	50
red 2	649	80
IR	733	20

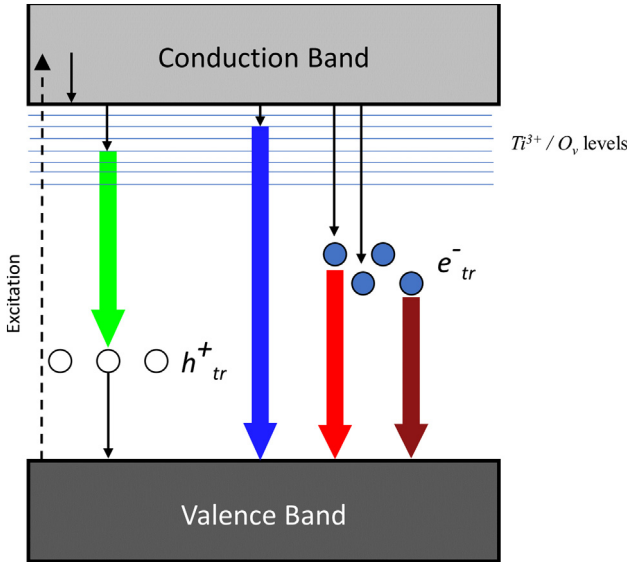

Fig. 10. Schematic representation of the localized states within the bandgap of the material. Black arrows indicate relaxation towards lower-energy states, while coloured arrows show radiation observed in photoluminescence measurements. The colours are adequate to those in Fig. 8. (For interpretation of the references to colour in this figure legend, the reader is referred to the web version of this article.)

CRediT authorship contribution statement

Jakub Wawrzyniak: Investigation, Formal analysis, Data curation, Validation, Visualization, Writing-orginal draft, Writing-review and editing. **: . Jakub Karczewski:** Investigation. **Piotr Kupracz:** Investigation. **Katarzyna Grochowska:** Conceptualization, Visualization, Resources, Writing - review & editing. **Karol Załęski:** Investigation. **Oleksandr Pshyk:** Investigation. **Emerson Coy:** Investigation. **Michał Bartmański:** Investigation. **Marek Szkodo:** Validation, Formal analysis. **Katarzyna Siuzdak:** Conceptualization, Writing - review & editing, Resources, Supervision, Project administration.

Declaration of Competing Interest

The authors declare that they have no known competing financial interests or personal relationships that could have appeared to

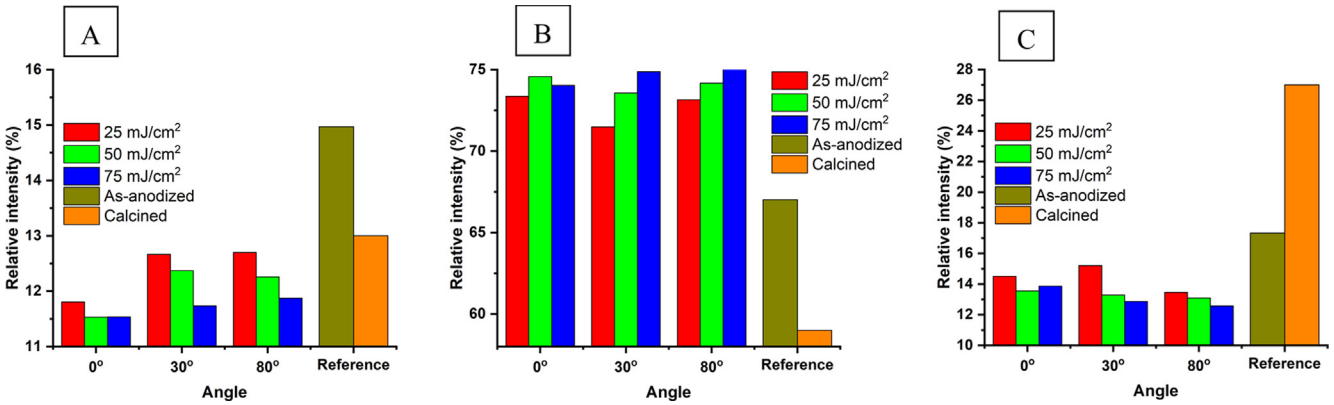

Fig. 9. The relative area of the red (A), green (B), and blue (C) emissions of the samples. (For interpretation of the references to colour in this figure legend, the reader is referred to the web version of this article.)

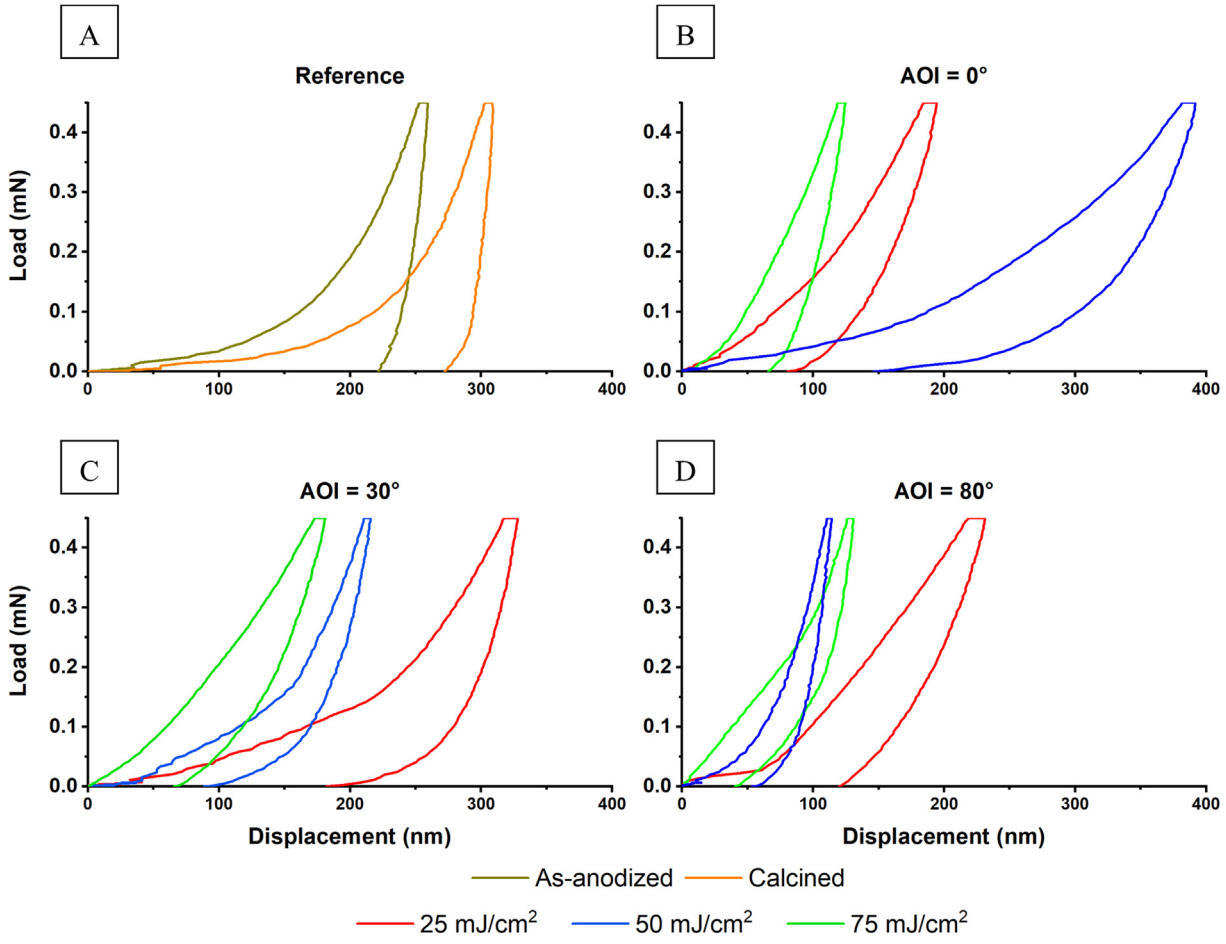

Fig. 11. Load-displacement curves for reference samples (A) and samples treated at normal angle of incidence (B), 30° (C), and 80° (D).

Table 3
Hardness and reduced Young's modulus for reference specimens and samples treated by the laser beam. H stands for hardness, E is a reduced Young's modulus and ± indicates standard deviation.

Angle [°]	0		30		80	
Energy density [mJ/cm^2]	H [GPa]	E [GPa]	H [GPa]	E [GPa]	H [GPa]	E [GPa]
25	0.49 ± 0.28	11.6 ± 6.3	0.16 ± 0.09	4.9 ± 2.06	0.43 ± 0.3	8.18 ± 5.04
50	1.03 ± 0.44	20.7 ± 4.9	0.56 ± 0.44	11.4 ± 6.1	0.65 ± 0.62	11.6 ± 9.6
75	0.20 ± 0.19	5.7 ± 5.6	0.57 ± 0.29	11.1 ± 4.2	1.7 ± 0.73	23.9 ± 9.6
Reference (as-anodized)		H = 0.470 ± 0.3, E = 15.6 ± 8.8				
Reference (calcined)		H = 0.19 ± 0.18, E = 11.1 ± 5.7				

influence the work reported in this paper.

Acknowledgements

This work received financial support from the Polish National Science Centre: Grant No. 2017/26/E/ST5/00416.

References

[1] J.S. Khaw, M. Curioni, P. Skeldon, C.R. Bowen, S.H. Cartmell, A novel methodology for economical scale-up of TiO_2 nanotubes fabricated on Ti and Ti alloys, J. Nanotech. 2019 (2019) 1–13, https://doi.org/10.1155/2019/5902346.
[2] M. Paulose, H.E. Prakasam, O.K. Varghese, L. Peng, K.C. Popat, G.K. Mor, T.A. Desai, C.A. Grimes, TiO_2 nanotube arrays of 1000 μm length by anodization of titanium foil: phenol red diffusion, J. Phys. Chem. C. 111 (2007) 14992–14997, https://doi.org/10.1021/jp075258r.
[3] S. Ozkan, N.T. Nguyen, A. Mazare, P. Schmuki, Optimized spacing between TiO_2 nanotubes for enhanced light harvesting and charge transfer, ChemElectroChem 5 (2018) 3183–3190, https://doi.org/10.1002/celc.201801136.
[4] J. Kim, B. Kim, C. Oh, J. Ryu, H. Kim, E. Park, K. No, S. Hong, Effects of NH_4F and distilled water on structure of pores in TiO_2 nanotube arrays, Sci Rep. 8 (2018) 12487, https://doi.org/10.1038/s41598-018-30668-3.
[5] X. Kang, S. Chen, Photocatalytic reduction of methylene blue by TiO_2 nanotube arrays: effects of TiO_2 crystalline phase, J Mater Sci. 45 (2010) 2696–2702, https://doi.org/10.1007/s10853-010-4254-5.
[6] X. Wang, L. Sun, S. Zhang, X. Wang, Ultralong, small-diameter TiO_2 nanotubes achieved by an optimized two-step anodization for efficient dye-sensitized solar cells, ACS Appl. Mater. Interf. 6 (2014) 1361–1365, https://doi.org/10.1021/am404966e.
[7] L. Li, Z. Liu, Q. Zhang, C. Meng, T. Zhang, J. Zhai, Underwater superoleophobic porous membrane based on hierarchical TiO_2 nanotubes: multifunctional integration of oil–water separation, flow-through photocatalysis and self-cleaning, J. Mater. Chem. A 3 (2015) 1279–1286, https://doi.org/10.1039/C4TA04699D.
[8] B. Karunagaran, P. Uthirakumar, S.J. Chung, S. Velumani, E.-K. Suh, TiO_2 thin film gas sensor for monitoring ammonia, Mater. Character. 58 (2007) 680–684, https://doi.org/10.1016/j.matchar.2006.11.007.
[9] M. Benčina, I. Junkar, R. Zaplotnik, M. Valant, A. Iglič, M. Mozetič, Plasma-induced crystallization of TiO_2 nanotubes, Materials 12 (2019) 626, https://doi.org/10.3390/ma12040626.
[10] J. Yu, G. Dai, B. Cheng, Effect of crystallization methods on morphology and

photocatalytic activity of anodized TiO_2 nanotube array films, J. Phys. Chem. C 114 (2010) 19378–19385, https://doi.org/10.1021/jp106324x.
[11] A. John, M. Thankamoniamma, J. Puigdollers, R. Anuroop, B. Pradeep, T. Shripathi, R.R. Philip, Rapid room temperature crystallization of TiO_2 nanotubes, CrystEngComm. 19 (2017) 1585–1589, https://doi.org/10.1039/C6CE02526A.
[12] A. Casu, A. Lamberti, S. Stassi, A. Falqui, Crystallization of TiO_2 nanotubes by in situ heating TEM, Nanomaterials 8 (2018) 40, https://doi.org/10.3390/nano8010040.
[13] A. Lamberti, A. Chiodoni, N. Shahzad, S. Bianco, M. Quaglio, C.F. Pirri, Ultrafast room-temperature crystallization of TiO_2 nanotubes exploiting water-vapor treatment, Sci Rep. 5 (2015) 7808, https://doi.org/10.1038/srep07808.
[14] Y. Liao, W. Que, P. Zhong, J. Zhang, Y. He, A facile method to crystallize amorphous anodized TiO_2 nanotubes at low temperature, ACS Appl. Mater. Interf.. 3 (2011) 2800–2804, https://doi.org/10.1021/am200685s.
[15] C.K. Chung, S.L. Lin, S.Y. Cheng, K.P. Chuang, H.Y. Wang, Effect of sol–gel composition ratio and laser power on phase transformation of crystalline titanium dioxide under CO_2 laser annealing, Micro Nano Lett. 6 (2011) 494, https://doi.org/10.1049/mnl.2011.0133.
[16] J.S. Hoppius, D. Bialuschewski, S. Mathur, A. Ostendorf, E.L. Gurevich, Femtosecond laser crystallization of amorphous titanium oxide thin films, Appl. Phys. Lett. 113 (2018) 071904, , https://doi.org/10.1063/1.5027899.
[17] J. Kim, J. Kim, M. Lee, Laser welding of nanoparticulate TiO_2 and transparent conducting oxide electrodes for highly efficient dye-sensitized solar cell, Nanotechnology. 21 (2010) 345203, , https://doi.org/10.1088/0957-4484/21/34/345203.
[18] Y. Xu, M.A. Melia, L. Tsui, J.M. Fitz-Gerald, G. Zangari, Laser-induced surface modification at anatase TiO_2 nanotube array photoanodes for photoelectrochemical water oxidation, J. Phys. Chem. C. 121 (2017) 17121–17128, https://doi.org/10.1021/acs.jpcc.7b05368.
[19] M.-Y. Hsu, N. Van Thang, C. Wang, J. Leu, Structural and morphological transformations of TiO_2 nanotube arrays induced by excimer laser treatment, Thin Solid Films 520 (2012) 3593–3599, https://doi.org/10.1016/j.tsf.2011.12.036.
[20] M. Pavlenko, E.L. Coy, M. Jancelewicz, K. Załęski, V. Smyntyna, S. Jurga, I. Iatsunskyi, Enhancement of optical and mechanical properties of Si nanopillars by ALD TiO_2 coating, RSC Adv. 6 (2016) 97070–97076, https://doi.org/10.1039/C6RA21742G.
[21] Q. Zhang, L. Ma, M. Shao, J. Huang, M. Ding, X. Deng, X. Wei, X. Xu, Anodic oxidation synthesis of one-dimensional TiO2 nanostructures for photocatalytic and field emission properties, J. Nanomater. 2014 (2014) 1–14, https://doi.org/10.1155/2014/831752.
[22] V. Likodimos, T. Stergiopoulos, P. Falaras, J. Kunze, P. Schmuki, Phase composition, size, orientation, and antenna effects of self-assembled anodized titania nanotube arrays: a polarized Micro-Raman investigation, J. Phys. Chem. C 112 (2008) 12687–12696, https://doi.org/10.1021/jp8027462.
[23] M. Fernández-García, X. Wang, C. Belver, J.C. Hanson, J.A. Rodriguez, Anatase-TiO_2 nanomaterials: morphological/size dependence of the crystallization and phase behavior phenomena, J. Phys. Chem. C. 111 (2007) 674–682, https://doi.org/10.1021/jp065661i.
[24] X. Chen, S.S. Mao, Titanium dioxide nanomaterials: synthesis, properties, modifications, and applications, Chem. Rev. 107 (2007) 2891–2959, https://doi.org/10.1021/cr0500535.
[25] A.C. Ferrari, J. Robertson, Resonant Raman spectroscopy of disordered, amorphous, and diamondlike carbon, Phys. Rev. B 64 (2001) 075414, , https://doi.org/10.1103/PhysRevB.64.075414.
[26] A. Li Bassi, D. Cattaneo, V. Russo, C.E. Bottani, E. Barborini, T. Mazza, P. Piseri, P. Milani, F.O. Ernst, K. Wegner, S.E. Pratsinis, Raman spectroscopy characterization of titania nanoparticles produced by flame pyrolysis: The influence of size and stoichiometry, J. Appl. Phys. 98 (2005) 074305, , https://doi.org/10.1063/1.2061894.
[27] K.-H. Sun, Fundamental conditions of glass formation, J Am. Ceram. Soc. 30 (1947) 277–281, https://doi.org/10.1111/j.1151-2916.1947.tb19654.x.
[28] F.H. Stillinger, A topographic view of supercooled liquids and glass formation, Science 267 (1995) 1935–1939, https://doi.org/10.1126/science.267.5206.1935.
[29] D.R.G. Mitchell, DiffTools: Electron diffraction software tools for DigitalMicrograph™, Microscopy Res. Tech. 71 (2008) 588–593, https://doi.org/10.1002/jemt.20591.
[30] J. Tauc, Optical properties of amorphous semiconductors, in: J. Tauc (Ed.), Amorphous and Liquid Semiconductors, Springer, US, Boston, MA, 1974, pp. 159–220.
[31] A.S. Hassanien, A.A. Akl, Influence of composition on optical and dispersion parameters of thermally evaporated non-crystalline $Cd_{50\ S50-x}\ S_ex$ thin films, J. All. Comp. 648 (2015) 280–290, https://doi.org/10.1016/j.jallcom.2015.06.231.
[32] M. Janczarek, E. Kowalska, On the origin of enhanced photocatalytic activity of copper-modified titania in the oxidative reaction systems, Catalysts 7 (2017) 317, https://doi.org/10.3390/catal7110317.
[33] B. Bharti, S. Kumar, H.-N. Lee, R. Kumar, Formation of oxygen vacancies and Ti^{3+} state in TiO_2 thin film and enhanced optical properties by air plasma treatment, Sci. Rep. 6 (2016) 32355, https://doi.org/10.1038/srep32355.
[34] S. Mathew, A. Kumar Prasad, T. Benoy, P.P. Rakesh, M. Hari, T.M. Libish, P. Radhakrishnan, V.P.N. Nampoori, C.P.G. Vallabhan, UV-Visible photoluminescence of TiO_2 nanoparticles prepared by hydrothermal method, J. Fluoresc. 22 (2012) 1563–1569, https://doi.org/10.1007/s10895-012-1096-3.
[35] A. Stevanovic, M. Büttner, Z. Zhang, J.T. Yates, Photoluminescence of TiO2: effect of UV light and adsorbed molecules on surface band structure, J. Am. Chem. Soc. 134 (2012) 324–332, https://doi.org/10.1021/ja2072737.
[36] C. Mercado, Z. Seeley, A. Bandyopadhyay, S. Bose, J.L. McHale, Photoluminescence of dense nanocrystalline titanium dioxide thin films: effect of doping and thickness and relation to gas sensing, ACS Appl. Mater. Interf. 3 (2011) 2281–2288, https://doi.org/10.1021/am2006433.
[37] N.D. Abazović, M.I. Čomor, M.D. Dramićanin, D.J. Jovanović, S.P. Ahrenkiel, J.M. Nedeljković, Photoluminescence of anatase and rutile TiO_2 particles, J. Phys. Chem. B 110 (2006) 25366–25370, https://doi.org/10.1021/jp064454f.
[38] D.K. Pallotti, L. Passoni, P. Maddalena, F. Di Fonzo, S. Lettieri, Photoluminescence mechanisms in anatase and rutile TiO_2, J. Phys. Chem. C 121 (2017) 9011–9021, https://doi.org/10.1021/acs.jpcc.7b00321.
[39] W.-Y. Chang, T.-H. Fang, Z.-W. Chiu, Y.-J. Hsiao, L.-W. Ji, Nanomechanical properties of array TiO_2 nanotubes, Microporous Mesoporous Mater. 145 (2011) 87–92, https://doi.org/10.1016/j.micromeso.2011.04.035.
[40] Y.N. Xu, M.N. Liu, M.C. Wang, A. Oloyede, J.M. Bell, C. Yan, Nanoindentation study of the mechanical behavior of TiO_2 nanotube arrays, J. Appl. Phys. 118 (2015) 145301, , https://doi.org/10.1063/1.4932213.